



Oude Waalsdorperweg 63
P.O. Box 96864
2509 JG The Hague
The Netherlands

www.tno.nl

T +31 70 374 00 00

F +31 70 328 09 61

info-DenV@tno.nl

TNO report

TNO-DV 2008 A067

**Discriminating Sea Spikes in Incoherent Radar
Measurements of Sea Clutter**

Date	March 2008
Author(s)	Dr J. J. M. de Wit, MSc Dr M. W. Schouten, MSc
Classification report	Ongerubriceerd
Classified by	drs W. Pelt
Classification date	4 Februari 2008 (after 10 years this classification is no longer valid)
Title	Ongerubriceerd
Managementuittreksel	Ongerubriceerd
Abstract	Ongerubriceerd
Report text	Ongerubriceerd
Appendices	Ongerubriceerd
Copy no	6
No. of copies	20
Number of pages	33 (incl. appendices, excl. RDP & distribution list)

The classification designation Ongerubriceerd is equivalent to Unclassified, Stg. Confidencieel is equivalent to Confidential and Stg. Geheim is equivalent to Secret.

All rights reserved. No part of this report may be reproduced in any form by print, photoprint, microfilm or any other means without the previous written permission from TNO.

All information which is classified according to Dutch regulations shall be treated by the recipient in the same way as classified information of corresponding value in his own country. No part of this information will be disclosed to any third party.

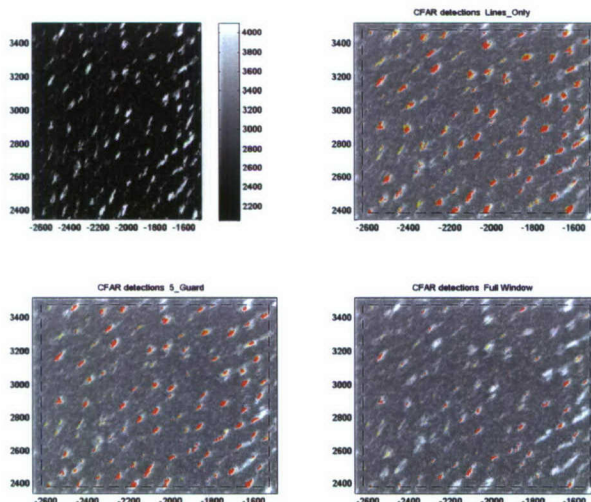
In case this report was drafted on instructions from the Ministry of Defence the rights and obligations of the principal and TNO are subject to the standard conditions for research and development instructions, established by the Ministry of Defence and TNO, if these conditions are declared applicable, or the relevant agreement concluded between the contracting parties.

© 2008 TNO

20080522123

Discriminating Sea Spikes in Incoherent Radar Measurements of Sea Clutter

Sinds 2002 ontwikkelt TNO speciale signaalverwerkingstechnieken om de functionaliteit van gewone navigatieradars uit te breiden. Een voorbeeld is de mogelijkheid om kleine oppervlaktedoelen te kunnen detecteren tegen een dynamische achtergrond, namelijk het zeeoppervlak. Het onderscheiden van zogenaamde *sea spikes* verdient hierbij speciale aandacht.



Probleemstelling

In opdracht van de Koninklijke Marine is de mogelijkheid om kleine of zwakke oppervlaktedoelen te detecteren met een navigatieradar onderzocht. Over het algemeen zullen de resolutie en de gevoeligheid van een radar verbeterd moeten worden om kleine(re) doelen te kunnen detecteren. Voor hogere resoluties speelt echter de radarverstrooiing aan het zeeoppervlak een belangrijke rol in het detectieproces: de verstrooiing aan kleine doelen kan te laag zijn om boven de *zeeclutter* uit te komen. Daarnaast kan het optreden van zogenaamde *sea spikes* leiden tot vele valse detecties. Een *sea spike* is een plotselinge, kortstondige piek in de

zeeclutter. Het ontstaan van *sea spikes* wordt van oudsher in verband gebracht met brekende golven. Dus vooral in relatief ondiepe kustwateren kunnen veel *sea spikes* optreden.

Beschrijving van de werkzaamheden

Er is een literatuuronderzoek uitgevoerd om de onderscheidende eigenschappen van *sea spikes* te inventariseren. Daarnaast is onderzocht of het mogelijk is om *sea spikes* te kunnen detecteren met behulp van een gewone incoherente navigatieradar.

Resultaten en conclusies

Het zeeoppervlak is dynamisch en als gevolg daarvan varieert de radarverstrooiing aan het zeeoppervlak in de ruimte. In navigatieradars worden daarom *constant false-alarm rate* (CFAR) detectietechnieken toegepast. De detectiedrempel van een CFAR detector past zich aan aan de (lokale) intensiteit van de achtergrond. Om de detectiedrempel te kunnen berekenen moet een aanname gedaan worden met betrekking tot de amplitudeverdeling van de achtergrond.

Van oudsher worden Gaussische of Rayleigh-verdelingen gebruikt in het geval van zeeclutter. Voor hogere radarresoluties zijn deze verdelingen echter niet meer bruikbaar. Uit het literatuuronderzoek is gebleken dat, voor hogere resoluties, andere verdelingen, zoals de Weibull-verdeling of de *K*-distributie, geschikter zijn. Proeven met gemeten data tonen aan dat een 'Weibull-detector' inderdaad beter presteert dan een 'Gaussische detector'. Echter, het aantal valse detecties als gevolg van *sea spikes* blijft onveranderd te hoog.

Het is dus onwaarschijnlijk dat kleine doelen gedetecteerd kunnen worden op afstanden van 5 tot 15 km met een acceptabele *false-alarm rate* als geen onderscheid gemaakt kan worden tussen *sea spikes* en echte doeldetecties.

Dat onderscheid kan wellicht gemaakt worden door de karakteristieke eigenschappen van sea spikes te exploiteren. Karakteristieke eigenschappen van sea spikes zijn de plotselinge stijging van de polarisatieverhouding HH/VV en toename van de Dopplersnelheid. Let wel, dit zijn eigenschappen die typisch niet gemeten kunnen worden met een gewone incoherente navigatieradar.

Voor de volgende generatie navigatieradars wordt echter nadrukkelijk gekeken naar coherente systemen. Het is daarom de moeite waard om de toegevoegde waarde van coherente radardata voor het detecteren van sea spikes te onderzoeken. Een dergelijk onderzoek zal moeten beginnen

met een literatuuronderzoek gericht op coherente radarobservaties van zeeclutter en kleine doelen. Vervolgens kunnen speciale detectietechnieken ontwikkeld worden die de Dopplereigenschappen van sea spikes uitbuiten. Een voorwaarde voor het ontwikkelen en valideren van zulke nieuwe detectietechnieken is dat coherente radardata van zeeclutter en kleine doelen beschikbaar zijn.

Toepasbaarheid

Geschiktere modellen voor de amplitudeverdeling kunnen direct toegepast worden in CFAR-detectietechnieken. Het is echter niet te verwachten dat het gebruik van deze modellen zal leiden tot een werkbare false-alarm rate.

Contact en rapportinformatie

Oude Waalsdorperweg 63
Postbus 96864
2509 JG Den Haag

T +31 70 374 00 00
F +31 70 328 09 61

info-DenV@tno.nl

TNO-rapportnummer
TNO-DV 2008 A067

Oprachtnummer

-

Datum
maart 2008

Auteur(s)
dr. ir. J. J. M. de Wit,
dr. ir. M. W. Schouten

Rubricering rapport
Ongerubriceerd

PROGRAMMA	PROJECT
Programmabegeleider drs. W. Pelt, DMO\DWS&B\RZS\OBI	Projectbegeleider drs. W. Pelt, DMO\DWS&B\RZS\OBI
Programmaleider prof. dr. A.M.J. van Eijk, TNO Defensie en Veiligheid	Projectleider dr. ir. J.J.M. de Wit, TNO Defensie en Veiligheid
Programmatitel Omgevingsinvloeden op sensor- en wapensystemen	Projecttitel Clutter
Programmanummer V509	Projectnummer 032.10287
Programmaplanning Start 01-01-2006 Gereed 31-12-2008	Projectplanning Start 01-01-2006 Gereed 01-12-2008
Frequentie van overleg Er is diverse malen contact geweest met de projectbegeleider over de invulling en de voortgang van het onderzoek.	Projectteam ir. J.C.M. Kleijweg, dr. ir. J.J.M. de Wit, dr. ir. M.W. Schouten

Summary

The last years, naval tasks gradually changed to peacekeeping, prevention of terrorist attacks, and monitoring of piracy and drug traffic. At the same time, the area of naval operations shifted from open sea to littoral waters. These changes necessitate the capability to detect small vessels in the complex coastal environment.

Generally speaking, both the resolution and sensitivity of radars must be improved to aid the detection of small vessels. However, at high resolutions, the backscatter from the sea surface starts to play an important role in the detection process. In particular, the occurrence of sea spikes may significantly increase the false-alarm rate. The specific characteristics of spiking events must therefore be established in order to separate them from true target echoes.

The most distinct characteristics of sea spikes are the sudden increase in Doppler speed and polarization ratio. These characteristics cannot be measured with current ship navigation radars, but future navigation radars will be coherent. Thus, for future research, it is worthwhile to investigate the added value of using coherent sea clutter measurements.

At high grazing angles and low resolution, the sea clutter amplitude has a Rayleigh distribution. As a consequence, constant false-alarm rate detectors currently used are generally based on Rayleigh distributed signals. However, for high resolutions and low grazing angles, the sea clutter amplitude becomes quickly less Rayleigh distributed. Therefore, the performance of constant false-alarm rate detectors can be improved by using a more appropriate distribution model, such as the Weibull distribution or the K -distribution.

Contents

1	Introduction	7
2	Characteristics of Sea Clutter and Spikes	9
2.1	Origin of Sea Spikes	9
2.2	Sea Clutter Polarization Dependency	10
2.3	Sea Clutter Wind Dependency	13
2.4	Sea Clutter Amplitude Distribution	15
2.5	Discriminating Sea Spikes	18
3	The Ships Radar Concept	22
3.1	Data Sets	23
3.2	Discriminating Sea Spikes with SHIRA	23
3.2.1	Current Processing of Data Patches at Near-Range	23
3.2.2	Processing of Data Patches at Long-Range	26
4	Conclusion	30
5	References	31

Abbreviations

CFAR	Constant False-Alarm Rate
CST	Composite Surface Theory
FFT	Fast Fourier Transform
PDF	Probability Density Function
DEKODO	Detectie van kleine oppervlakte doelen
FLIP	Floating Instrument Platform
HH	Horizontal transmit and horizontal receive polarization
HRZC	Hoge-Resolutie Zeeclutter
PRF	Pulse Repetition Frequency
PRI	Pulse Repetition Interval
PUT	Pixel-Under-Test
RCS	Radar Cross Section
SHIRA	Ships Radar
TNO	Netherlands Organisation for Applied Scientific Research
VV	Vertical transmit and vertical receive polarization

1 Introduction

Over the years, naval tasks gradually changed to peacekeeping, prevention of terrorist attacks, and monitoring of piracy and drug traffic. The area of naval operations shifted from open sea to littoral waters.

During the Cold War, naval radar systems were designed to monitor large areas of open sea at low spatial and temporal resolution to detect for instance frigates and aircraft carriers. The altered naval tasks necessitate the capability to detect coasters and other small vessels in the complex coastal environment. This has brought the Royal Netherlands Navy around to formulate new requirements for the next generation naval radar systems.

In order to support the Royal Netherlands Navy in this requirements definition, TNO initiated the research program "Detectie van kleine oppervlakte-doelen DEKODO" ("Detection of Small Surface Targets"). Under the umbrella of this program, several projects were started to develop novel filtering and detection techniques to aid the radar detection of small vessels.

Generally speaking, both the resolution and sensitivity of naval radars must be improved to aid the detection of small boats. However, at high radar resolutions, the backscatter from the sea surface or *sea clutter* starts to play an important role in the target detection process. The radar backscatter from small vessels may be too low to be discriminated from the sea clutter. Moreover, the occurrence of *sea spikes*, i.e. sudden increases in the radar backscatter from the sea surface, may significantly increase the number of false alarms.

In order to aid the detection of small targets against a background of sea clutter, existing models of radar sea clutter must be improved to reflect the sea clutter in littoral waters; as a minimum spiking events must be included. Moreover, temporal and spatial correlation of sea clutter and typical characteristics of sea spikes may be exploited in detection and tracking algorithms.

Within the framework of DEKODO, a novel sea clutter filter has been developed. This filter makes use of a series of radar measurements and the *wave dispersion relation* to estimate the sea clutter in the successive measurements [1]. The clutter filter works well when the wave field is clearly observable in the radar measurements. This is the case for short ranges up to 2 or 3 km (i.e. high grazing angles). For large ranges, the grazing angle becomes very small and, due to shadowing, only the wave crests are visible occasionally, see Figure 1.1. Therefore, at larger ranges, the performance of the clutter filter deteriorates. Moreover, the filter cannot predict the occurrence of sea spikes.

In addition, the projects "Toepassing model hoge resolutie zeeclutter HRZC"

("Application of the High Resolution Sea Clutter Model") and "Radar-zogdetectie"

("Radar Detection of Wakes") were completed under the umbrella of DEKODO. Within the framework of HRZC, an improved sea clutter model including spiking events has been developed [2]-[4]. With the aid of this numerical model, statistics of sea clutter and sea spikes can be obtained. These statistics are an essential help in designing adapted constant false-alarm rate (CFAR) detectors.

Within the project "Radar zogdetectie" a detection technique has been developed that exploits a vessel's V-wake [5], [6]. The V-wake detector works well, but the performance depends highly on the visibility of the V-wake. Thus obviously, a V-wake detector is not able to detect stationary vessels and furthermore its performance depends on target range and radar aspect angle.

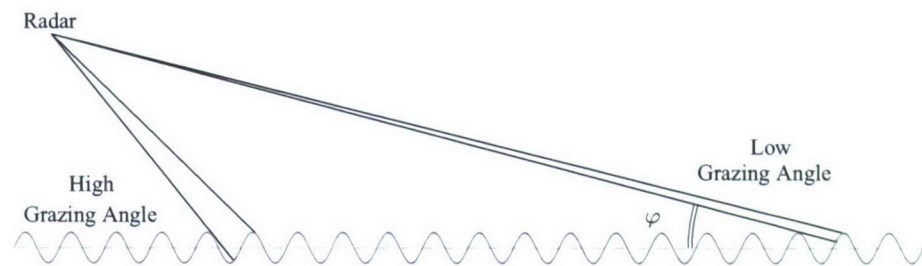


Figure 1.1 The effect of grazing angle φ on the observability of a wave field; at shallow grazing angles, only the wave crests are observable due to shadowing by the preceding wave crest.

As discussed above, the clutter filter and the V-wake detector work very well for relatively short ranges; up to 2 to 3 km. However, one of the requirements newly formulated by the Royal Netherlands Navy is the ability to detect small vessels at ranges up to 15 km. For the region between roughly 5 and 15 km, novel processing techniques to reduce the impact of sea clutter and in particular spiking events must be developed. Such techniques may exploit special characteristics of sea spikes and possible spatial or temporal correlations of spiking events [7]. The development of these processing techniques is carried out under the umbrella of the aforementioned HRZC project.

An additional objective of the HRZC project is to investigate the feasibility of using the novel processing techniques with standard ship navigation radar systems. Long-haul trade vessels and inland boats are usually equipped with navigation radar. Extension of the capabilities of such radars is favorable for several reasons. For instance, a better capability to detect small targets, improves safety. Especially in coastal waters, large lakes, and rivers where many small boats and yachts are present, which themselves may not have radar or beacons.

In the following chapter, an introduction to radar backscatter from the sea surface and sea spikes will be given. An extensive literature research has been conducted to investigate the properties of sea clutter and in particular spiking events. The chapter will be completed with a summary of possibilities to separate sea spikes from other detections. In Chapter 3, the operation, data acquisition, and signal processing of a typical navigation radar will be discussed. In addition, the capability of distinguishing sea spikes from other radar detections will be explored. The report will be completed with the conclusion and recommendations.

2 Characteristics of Sea Clutter and Spikes

In this chapter, the results of a literature research on the properties of sea clutter and sea spikes will be presented. At the end of the chapter, possibilities to discriminate spiking events from other detections will be discussed.

2.1 Origin of Sea Spikes

At moderate grazing angles, the microwave backscatter from the sea surface is reasonably well described by the *composite surface theory* (CST). This theory describes the sea surface as small Bragg-resonant capillary waves riding on top of heaving long gravity waves [8]. The backscatter from the small capillary waves, the *Bragg scatter*, is the dominant backscatter mechanism at radar frequencies. The long underlying waves can be resolved through the modulation of the Bragg scatter. This modulation is primarily caused by the locally varying angle of incidence.

However, at low grazing angles, i.e. of the order of 8° or smaller, strong peaks in the radar backscatter are frequently observed, especially for HH-polarization.

These backscatter peaks, or sea spikes, can not be explained with the composite surface theory. Over the years, sea spikes have been associated with breaking waves and whitecapping, but an exhaustive theory of the backscatter processes giving rise to spiking events is still lacking. Different backscatter processes, such as edge diffraction and multipath reflection, have been suggested [9], [10].

The process of wave breaking starts with the wave profile becoming increasingly asymmetrical. The front-face of the crest steepens, eventually getting nearly vertical, whereas the trough maintains its original smooth shape, see Figure 2.1(a).

Simultaneously, a small jet forms at the top of the crest. Throughout the breaking process this jet grows and eventually plunges downward into the wave front, see Figures 2.1(b) and 2.1(c). When the jet plows into the wave front, air is entrained and water droplets are thrown upward. The plowing ends in strong underwater turbulence, which slowly diminishes leaving a less turbulent scar, see Figure 2.1(d).

The wave-breaking process is described in detail in e.g. [11], [12].

The different stages of the wave-breaking process can be distinguished in the radar backscatter due to strong variations in radar cross section (RCS), polarization ratio¹, and Doppler speed. The steepening of the wave crest is characterized by a rapid increase of the RCS and the polarization ratio. The RCS rises to 10 to 15 dB above the background level, whereas the polarization ratio increases to around 0 dB (background values are between 0 and -10 dB). At the same time, an increase in the Doppler speed occurs. When the wave front further steepens, the RCS for HH-polarization rises another 10 dB, resulting in a polarization ratio of about 5 dB. The Doppler speed increases to approximately $0.8c_0$ [12]; c_0 being the linear wave speed defined as

$$c_0 = \sqrt{\frac{g\lambda}{2\pi}}, \quad (2.1)$$

in which g is the acceleration due to gravity and λ is the length of the ocean waves.

Note that (2.1) is valid if the water depth is much larger than the wavelength.

Peak values for the RCS and polarization ratio occur during the plunging jet stage.

Polarization ratios over 25 dB have been observed [12]. Throughout this stage, the Doppler speed remains at about $0.8c_0$, although it sometimes increases to c_0 .

In the plowing stage, the HH-polarized and VV-polarized backscatter decorrelates.

1. The polarization ratio is defined as the ratio of the HH-polarized backscatter intensity to the VV-polarized backscatter intensity.

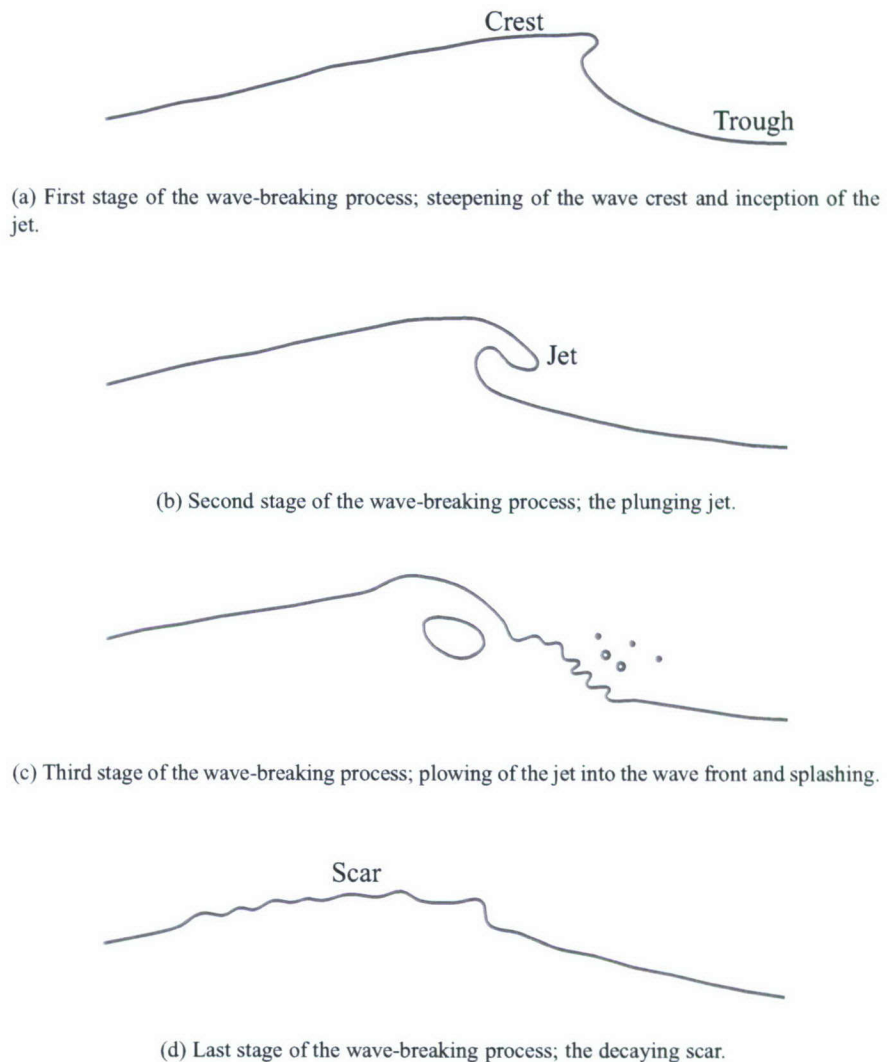


Figure 2.1 Wave profiles throughout the breaking process.

The Doppler speed for HH-polarization remains around c_0 , whereas the Doppler speed for VV-polarization falls off later in the plowing stage.

In the final stage, the RCS slowly returns to the background values (a little faster for HH-polarization). The polarization ratio returns to values between 0 and -10 dB and the Doppler speed drops.

2.2 Sea Clutter Polarization Dependency

Radar reflectivity of the ocean surface depends on of the polarization of the radar signal. The polarization ratio is often used as an indicator of sea spikes.

At high incidence (low grazing) angles, CST and Bragg scattering theory predict about 20 to 30 dB less backscatter for HH-polarization than for VV [4].

Moreover, observations show that whereas VV-polarized backscatter remains consistent with CST, HH-polarized backscatter becomes prone to spiking events and these spikes often have a polarization ratio larger than 1. Several effects, most of which deal with the geometric details of waves interacting with the wind, have been proposed to explain this

asymmetry of the sea spikiness. The dominant effects seem to be breaking waves, the occurrence of steep patches of the ocean surface causing a specular reflection towards the radar, and highly curved wave patches where signals are concentrated towards the radar. For target detection on relatively short ranges, HH-polarization seems to be the most desirable mode, as sea clutter is relatively low with respect to VV-polarization. Past experience within DEKODO has shown that the sea clutter within the first two to three kilometers from the radar can in many cases effectively be further reduced as the long gravity waves can be individually monitored and their propagation is rather predictable [1].

At lower grazing angles, however, where the signal becomes dominated by sea spikes rather than by well-behaved long-wave clutter, the HH-polarization of the conventional navigation radar system becomes a disadvantage due to dominance of HH-polarized backscatter in sea spikes.

The IPIX Dartmouth Database

In November 1993, a large database of high resolution radar measurements was collected using the McMaster IPIX radar at the east coast of Canada, from a cliff top near Dartmouth, Nova Scotia. The observations were made with a fully coherent X-band dual polarization radar. The dataset is fully documented and partially available from the website at <http://soma.ece.mcmaster.ca/ipix/dartmouth/>.

We show some of their observations where a small target was placed in the ocean.

The McMaster IPIX radar has a *stare* mode which scans a small portion of the azimuth circle, and which was centered on the target to provide high temporal resolution (1 kHz) measurements of a small target in sea clutter. We only use datasets that contain over 120 s of continuous observations.

As standard navigation radars are incoherent, we use just the amplitude information.

We do however compare VV and HH-polarized measurements. In the first example, a small target was located at a distance of about 2700 m in rather strong wave field with waves of about 2 m, see Figure 2.2.

That sea clutter is strong at the VV-polarization. Individual waves can be clearly tracked as they roll in from the ocean towards the radar. At HH-polarization, some of the wave fronts are still recognizable, but much weaker than at VV. The target is of comparable strength, which gives it far better visibility in the HH-polarized measurements.

The target is not continuously present, due to shadowing by the wave crests and multipath effects.

The one occasion in the Dartmouth IPIX database with a sample target located farther away is a series of observations of the same day, half an hour later. A target is present at a distance of about 5570 m, see Figure 2.3. Again, we can clearly track the individual waves in the VV-polarized data, but not quite as well in the HH. The target is, however, quite invisible in both datasets. Without prior knowledge, most of the peaks in especially the HH data should be considered a possible target.

Several other datasets are summarized in Figure 2.4. Here we show in the six upper panels the mean backscatter from a region of about 200 m, centered at the target which is around 2600 m away in all these cases. The solid lines denote the VV-polarized data, the dashed lines the HH, confirming the general picture of Figures 2.2 and 2.3. In all these cases, the target (at the center position of the horizontal axes) is marked by a clear maximum in backscatter of similar strength in both HH and VV. The clutter from waves is in all but one of the cases stronger in VV. The lower panel is the similar averaged field containing the remote target depicted in Figure 2.2.

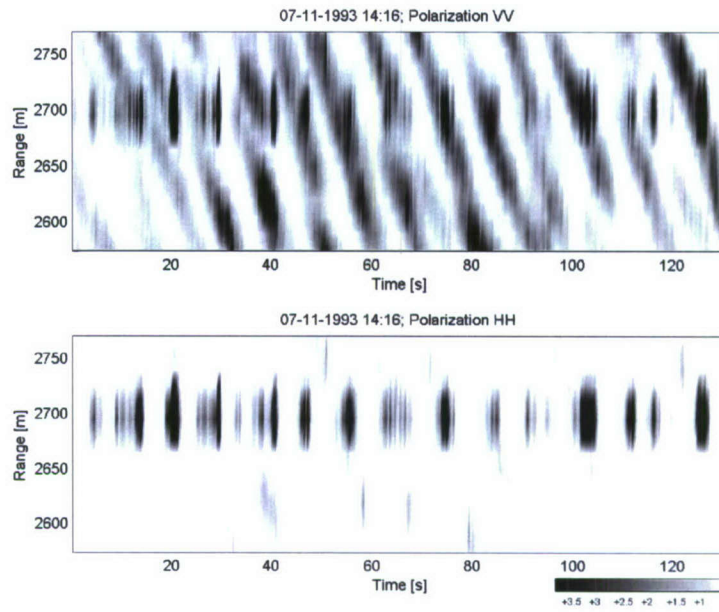


Figure 2.2 IPIX measurements of a small target at about 2700 m range at VV-polarization (upper panel) and HH-polarization (lower panel).

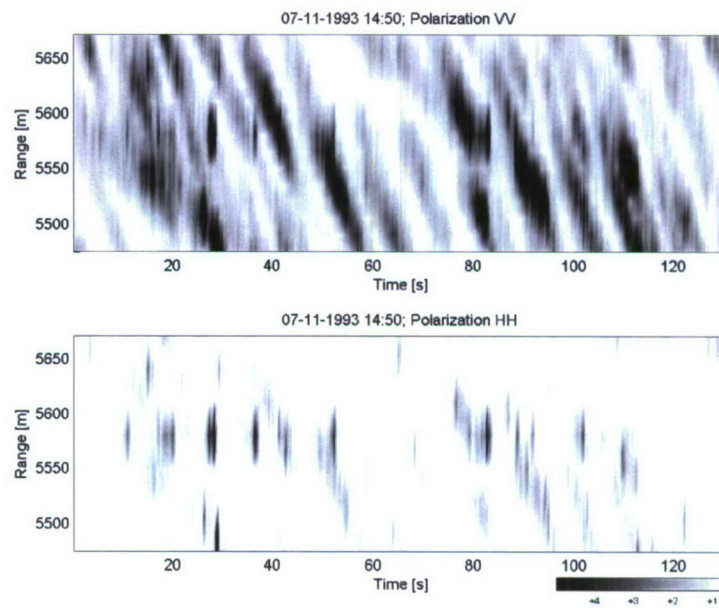


Figure 2.3 IPIX measurements of a small target at approximately 5570 m range at VV-polarization (upper panel) and HH-polarization (lower panel).

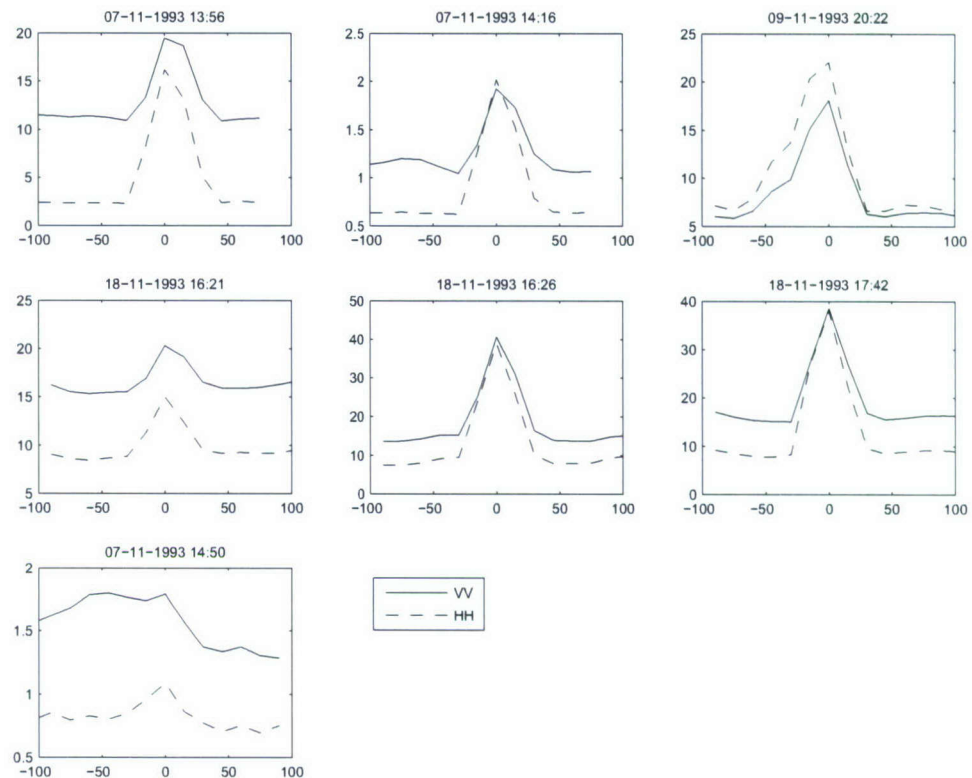


Figure 2.4 The mean radar backscatter measured by IPIX in an area around the target. The mean backscatter at VV-polarization (solid) and at HH-polarization (dashed) is shown.

2.3 Sea Clutter Wind Dependency

As the main driving force of the ocean, the wind is of obvious importance in the observation of sea surface. The relationship between radar backscatter and wind direction is however far from trivial. Without the presence of long surface waves, there seems to be a rather strong dependence on the azimuth relative to the wind. The strongest clutter signal is found when looking up-wind. The weakest clutter is found either in the cross-wind or down-wind direction, depending on the sea surface conditions and radar configuration [13], [14].

In [15] a HH-polarized X-band radar is tested for backscatter directionality with respect to the wind over quiet water (no long waves) in a sheltered lagoon off the German Baltic coast. Strongest backscatter looking in the upwind direction, dropping sharply around 90° (cross-wind) by about 30 dB. In this case, the weakest clutter appeared in the down-wind direction.

In contrast, in [14] observations south of Australia where again the strongest clutter signal is in the up-wind direction, but here a secondary maximum is found down-wind, with two minima in the cross-wind directions. Similar results are found for HH and VV-polarizations. In [14] the spikiness of the data is also estimated by fitting long-tailed distributions (the Weibull and K -distributions), but no dependence of the shape of the distributions on azimuth was found. It should be noted that his observations are at high grazing angle (i.e. 50 - 70°), and in such cases spikiness is likely of a different nature than that caused by the sea spikes at low grazing angle.

The presence of long waves or swell modifies this picture. These waves not only depend on local and present-time wind forcing, but also on wind events that are more remote both in time and place. Often, there is a dominant direction of incoming swell.

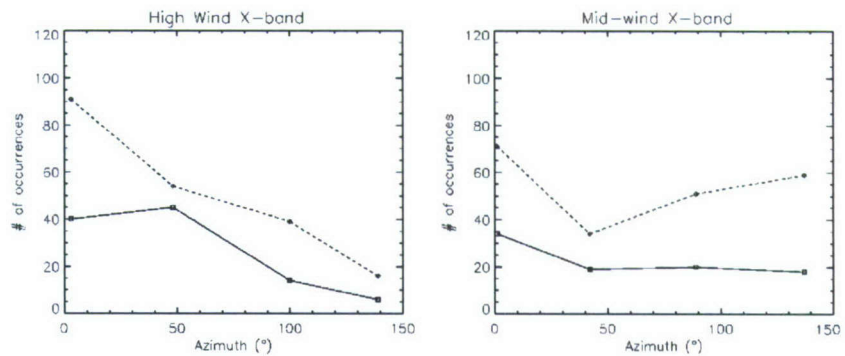


Figure 2.5 In some cases, sea spikes show a clear azimuthal dependence with respect to the wind. In a rather high wind case (left panel), 20 minutes of sea clutter observations [17] found significantly more sea spikes looking in the up-wind direction, both for HH (solid lines) and VV (dashed lines) polarizations. In a lower wind case, however, no such relation was found (right panel). Reproduced from [17]

Many observations are made from cliff tops overlooking the ocean, and for such coastal sites this would naturally be the direction towards open sea. There is some evidence for stronger HH-polarized sea spike behavior in the upwind direction (e.g. [16]), although this is based on a distinct location (South England cliff top).

A source of systematic observations of sea spikes and breaking waves on open water comes from several experiments performed with the Floating Instrument Platform (FLIP) operated from San Diego. These experiments are mostly conducted off the U.S. West coast, where swell is mostly from the Pacific (West). During the Coastal Ocean Probing Experiment (1995) large series of concurrent radar sea clutter and video observations were collected with FLIP near Northern Oregon.

More spikes are observed when looking into the wind (azimuth = 0) in the high wind case (10 m/s, Figure 2.5 left panel). However, no relation between spike occurrence and azimuth with respect to the wind is observed in a case with lower wind speed (6 m/s, Figure 2.5 right panel) [17]. In this location, not much whitecapping was observed, but spikes would coincide with locations of steep curvature of the waves, either from straight-on swell (Figure 2.6 left panel) or at the crossing of two waves coming from different directions (Figure 2.6 right panel) [17]. In this case, the direction of the waves would be the determining factor, not the direction of the wind.

A similar conclusion was reached for a dataset obtained in Eastern Canada overlooking the Atlantic (the aforementioned IPIX radar) [18].

In conclusion, we may state that the strongest radar returns are generally collected from the up-wind direction, but that the spikiest returns are expected in the up-swell direction. However, these are rules of thumb that have little predictive power in real-life situations. Details of the local setting (wind, waves, bottom and coastal geometry) can strongly modify the picture.

2.4 Sea Clutter Amplitude Distribution

In the present DEKODO signal processing, a simple CFAR algorithm based on a Gaussian distribution is applied: pixels are detected which have a backscatter intensity above a certain number (adjustable) of standard deviations above the mean. The standard deviation (σ) and mean (μ) are determined locally, by a number of cells around the pixel-under-test (PUT). To avoid contamination of the distribution by the possible target itself, the PUT and its immediate neighbors are not considered in the determination of the mean and variance. This standard CFAR practice has been applied rather extreme in the present DEKODO processing: the mean and standard deviation are determined by single lines of pixels a number of pixels away from the PUT. The size of this square region over which the distribution is estimated, can also be adjusted. For a standard setting of 10 pixels, this leads to an estimate of the distribution based on 80 pixels, at a distance of 10 pixels to the north, east, south and west of the PUT.

Clearly, the assumption of a Gaussian amplitude distribution is a very poor one in the context of spiky sea clutter. By no means does the Gaussian distribution fit observed distribution of received backscatter. For higher grazing angles, and lower radar resolution, the Rayleigh distribution has been traditionally used and found to fit well to observations [19]. There also seems to be a physical justification for Rayleigh amplitude distribution in such cases, as the in-phase and quadrature components are both Gaussian distributed.

For low grazing angles and high radar resolution, the received signal becomes increasingly spiky so that the *tail* of the distribution becomes significantly longer. The Rayleigh distribution fails to accommodate such *long-tailed* or spiky distributions. Other distributions that have been proposed and investigated in the context of high resolution low grazing angle radar observations of sea clutter are the log-normal, the Weibull, and the K -distribution. The Weibull and K -distributions behave rather similar in the tail region of the distribution, although the K -distribution seems to best capture this tail for HH polarized spiky clutter data [18], [20]. It is also the only one for which a physically meaningful explanation can be given, as it can be considered to be a compound distribution, originating in a Rayleigh distributed (high frequency) clutter field, the *speckle*, modulated by a low-frequency gamma-distributed field which may represent the underlying swell [21], [22].

As estimating the parameters of the K -distribution is a non-trivial undertaking [23], we have made a first effort to improve the CFAR algorithm by applying a Weibull distribution CFAR detector to a single snapshot of sea clutter and compared the results to the original detection algorithm implemented in the DEKODO signal processing.

We use a small region of the best medium distance dataset currently available, which was recorded on September 21, 2004 (listed as data set 1 in Table 3.2). A histogram of all radar backscatter data within a 256x256 pixel field of a randomly chosen revolution (Figure 2.7), shows the non-Gaussian nature of the underlying probability density function. Added to this figure are a Weibull fit to the observed data (solid line) and a Gaussian fit (dashed line). Both distributions are not very successful in capturing the spikiness of the data, as in both cases the tail is rather short, but there is a clear improvement when a Weibull distribution is used in the fit. In this scenario, all data are accumulated into one fit, so no local distributions are estimated. In the CFAR detection runs we show below, the distributions are defined locally, to allow for spatial inhomogeneity of the distributions. For this accumulated example, the 3σ Gaussian threshold would be at 3577, and be exceeded in 3% of the cases (1850 pixels). The corresponding threshold of the Weibull distribution would be at 3266, and be exceeded by 5% of the pixels. For a perfect fit of either distribution to the data, this percentage should be 0.13%, which sets the 3σ level of the Gaussian distribution.

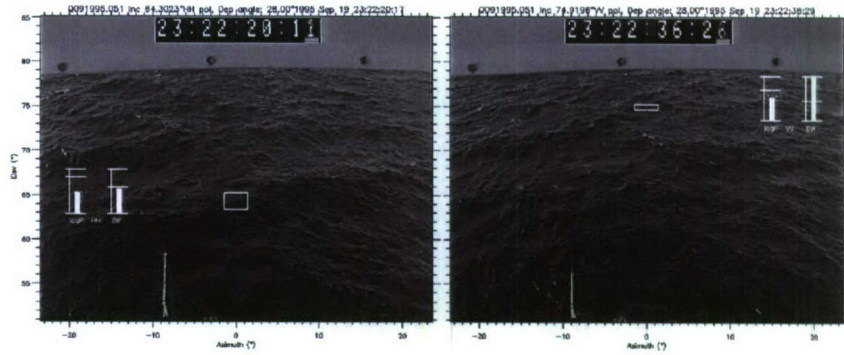


Figure 2.6 Two video stills, with the square denoting the patch of sea surface producing a strong spike in the radar backscatter. In the left panel, the high backscatter seems to result from looking into a steep wave patch. In the right panel, the crossing of two waves from different directions results in a highly curved surface strongly reflecting the radar signal.

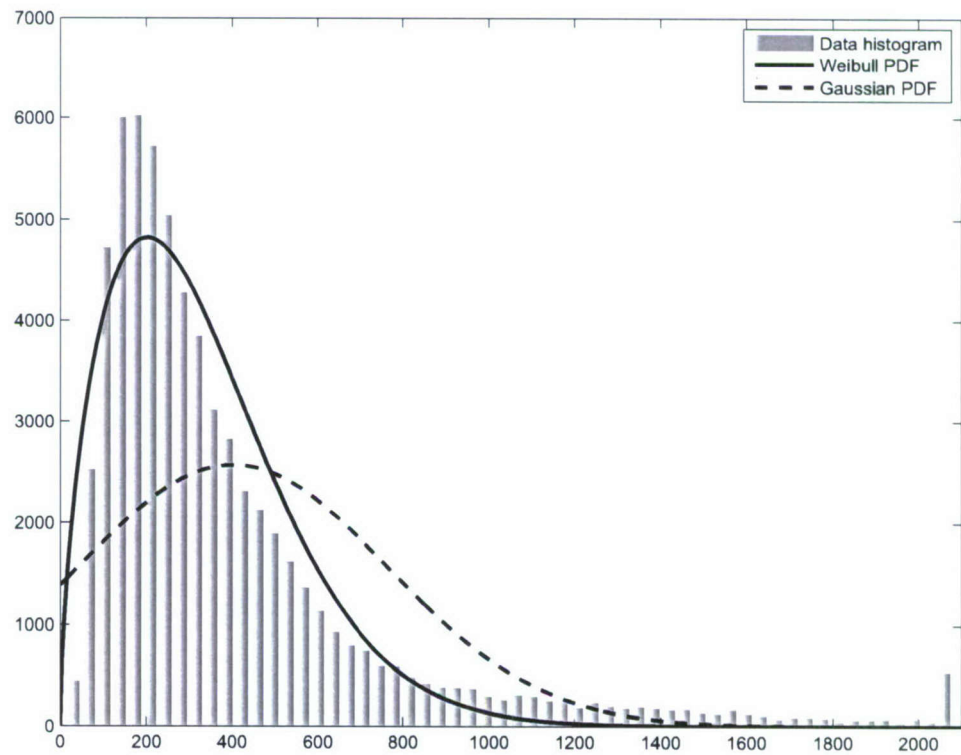


Figure 2.7 Backscatter intensities for 256x256 pixels in one sample for a 1x1 km region near Noordwijk, are shown here in a histogram. The probability density function estimated by a Weibull (solid line) and Gaussian (dashed line) fit are drawn as well. The last bin contains a relatively high number of points.

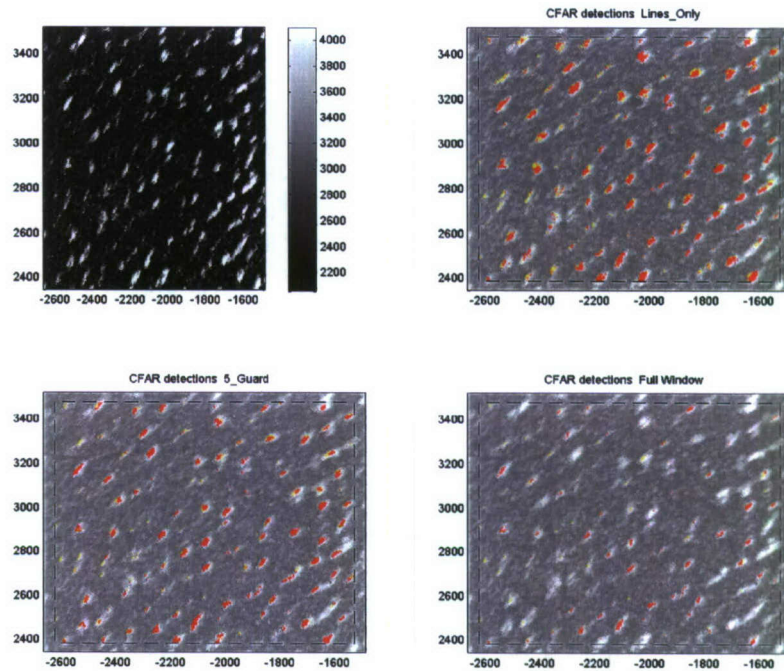


Figure 2.8 The sea clutter field of the upper left panel is subjected to different CFAR algorithms. Shown in red are the detections made by a Weibull estimate of the underlying distribution, in yellow those of a Gaussian distribution. Three options for choosing the pixels which contribute to the estimate are tested: a square of a single line at 10 pixels distance from the PUT (upper right); the 20x20 window centered on the PUT but with a 10x10 guard cell region blanked out to reduce the influence of the PUT and its immediate neighbors (lower left); the full 20x20 pixel window.

Table 2.1 Results CFAR.

Method	# Clusters Found	
	Gaussian	Weibull
Full Window	86	50
5 Guard	114	94
Single Lines	107	90

However, the real test is in the local CFAR estimates. Three setups have been tested for the determination of the local distribution parameters, as the Weibull distribution may become better defined when a larger number of neighboring points are evaluated. First, we apply the standard setup with 80 points in single lines at a distance of 10 pixels in each direction from the PUT, then a full window of 10 pixels in each direction is tested, and finally an intermediate setup with 5 guard cells in each direction. The number of clusters is reduced in all cases, see Table 2.1, which shows the potential of a more realistic probability distribution function (PDF) estimation as a way to reduce the number of false alarms. In Figure 2.8 we show the detections made by both estimators (Gaussian in yellow, Weibull in red). Clearly, in the *full window* case, the PUTs and their immediate neighbors have too much impact on the estimate of the distribution, which leads to non-detection of larger targets. This is also the case in which the number of clusters is most reduced.

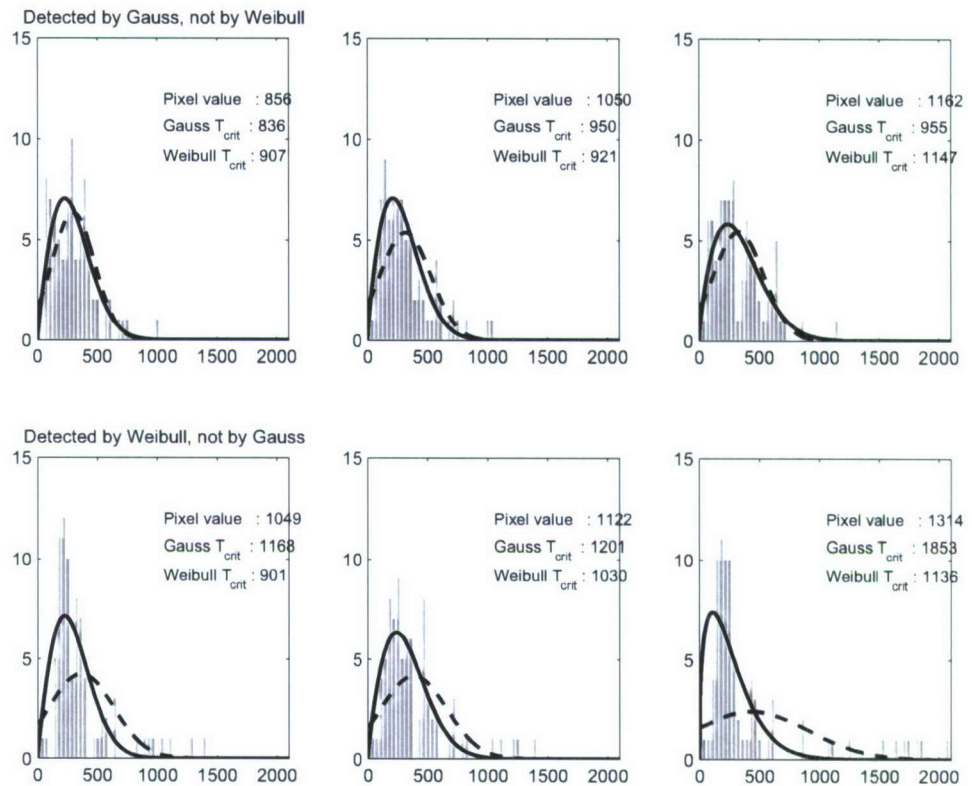


Figure 2.9 Six examples of local estimates of the PDF by consideration of a single line of points around the PUT. The histograms show the distribution of points surrounding a PUT. The Weibull (solid line) and Gaussian (dashed line) PDF approximations lead to different threshold values for detection. In the upper three cases, the pixel is detected by the Gaussian estimator, and rejected by the Weibull. In the lower three panels, the reverse is true.

In Figures 2.9 and 2.10, we see series of six cases in which one of the estimators led to a detection and the other did not. Here, we can also estimate the quality of the estimates of the PDFs. For the single line case, the PDFs are not very well defined due to a lack of data (80 points).

2.5 Discriminating Sea Spikes

The main problem of sea spikes is that they may significantly increase the number of detections. In common target detection processes, the radar detections are clustered and then fed to a tracker system. In principle, a tracker has to associate every cluster to an existing track or initiate a new track on that cluster. When the tracker is overfled with detections, it is, at the very least, no longer capable of real-time operation. In order to relieve the tracker system, the number of detections fed to the tracker has to be limited. Thus the radar system must estimate the (conditional) probability of a detection being a sea spike. In the estimation of this probability, many types of variables and information from different sources can play a role, as will be discussed in the following paragraphs.

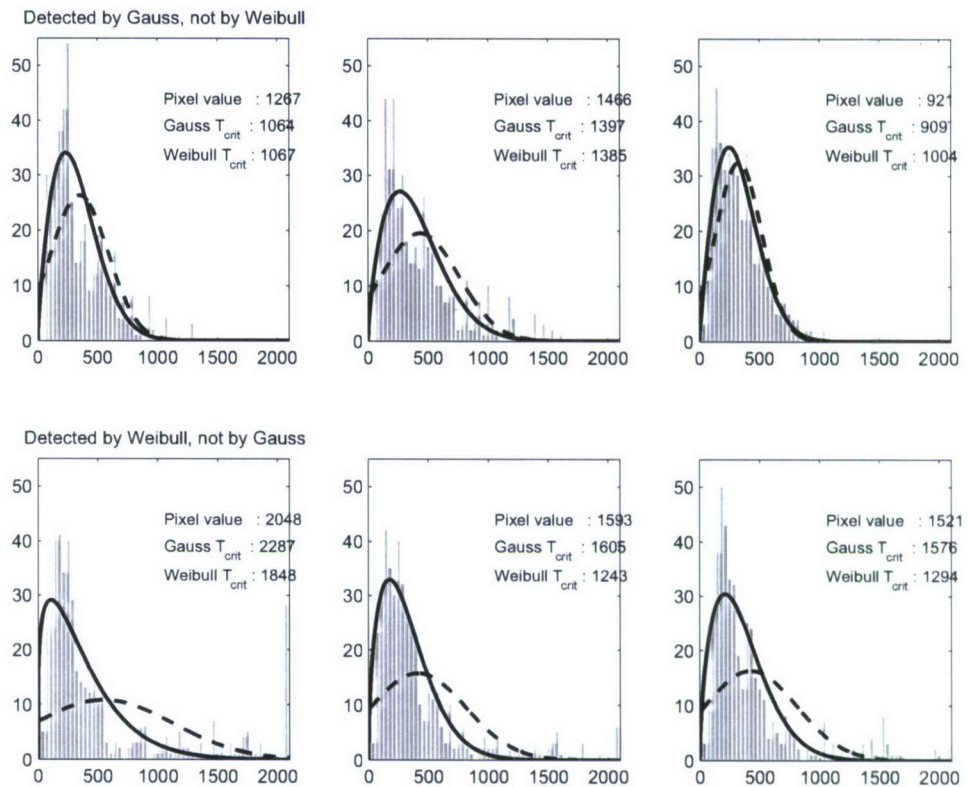


Figure 2.10 As Figure 2.9, but now the full 20x20 pixel window around the PUT is used to estimate the distribution.

Statistical, Polarimetric, and Doppler Properties

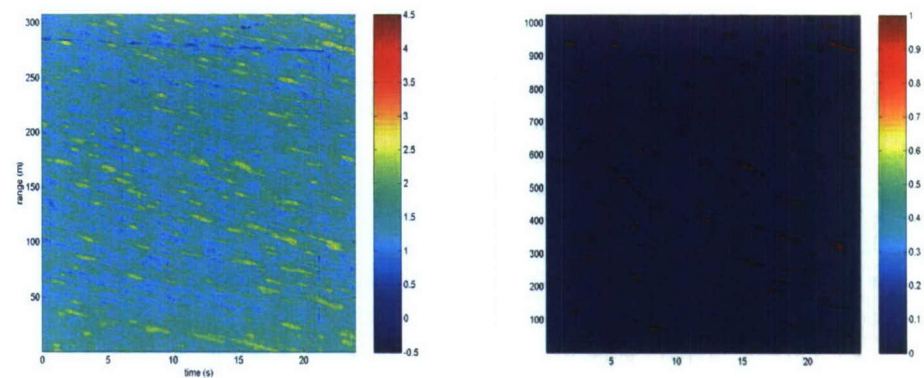
With appropriate statistical information of the radar backscatter, i.e. the underlying distribution, the CFAR detector parameters can be optimized. As was shown in Section 2.4, the performance of a CFAR detector based on the appropriate distribution is better than the performance of a basic Gaussian CFAR detector.

The most distinct characteristics of breaking waves and sea spikes are the sudden increase in HH-polarized backscatter, polarization ratio, and Doppler speed.

Earlier research already showed that these characteristics are indeed robust features to discriminate sea spikes [24]. In Figure 2.11(a) a sample image is shown of HH-polarized radar sea clutter. In this image, detections due to spiking events were separated by setting lower limits to the polarization ratio ($HH/VV > 0$) and the HH-polarized Doppler velocity ($v_d > 2 \text{ ms}^{-1}$). The outcome is depicted in Figure 2.11(b). As can be seen, a significant number of detections due to spiking events have been separated.

Spatial and Temporal Correlation

Spiking events exhibit spatial and temporal correlation, which may be exploited in the discrimination process [25]. Because spiking events occur at wave crests, they show up in radar images as long stretched structures up to several meters long, which lie parallel to the wave field. This is confirmed by Figure 2.11(b); the detected sea spikes come out as linear structures parallel to the crests of the dominant waves [24]. Moreover, sea spikes move with the waves at the same speed and in the same direction [26]. The size, orientation, and velocity of clusters of detections can be extracted from a series of radar images, when they are tracked from image to image. Consequently, the motion and orientation of the clusters can be weighted against the wave direction and wave period. When the clusters move with the waves, the detections are most likely sea clutter.



(a) The HH-polarized radar sea clutter image.
The color bar denotes amplitude in dB.

(b) The detected spiking events.

Figure 2.11 An example of HH-polarized sea clutter and the detected spiking events when lower limits are set to the polarization ratio and Doppler velocity.

In practice however, small targets are primarily observable when they are situated on wave crests. When they are in wave troughs they are practically undetectable due to shadowing. Therefore, in radar images, detections of small targets will be within the structures of clutter detections and they will appear to move with the wave crests as well.

Environmental and Atmospheric Variables

The assessment of the overall probability of wave breaking taking place may support the tracker. For that purpose a wave breaking criterion should be established. In literature, consensus has been reached that the steepness of waves cannot exceed a certain value. Waves which are steeper are unstable and will break. Wave steepness is defined as ak , where a is the wave's amplitude and k is the wave number [4]. The wave number can be extracted from radar data, but the wave height has to be delivered by an external source. Furthermore, wave breaking and thus sea spikes are more likely to occur at higher sea states. In addition, the probability that small vessels, such as dinghies, are at open sea under such conditions is relatively small. Also the wind and wave direction relative to the radar line-of-sight affect the probability of spiking events taking place. Knowledge of the local bottom topography can also be used to assess the overall probability of wave breaking taking place. One could think of an overlay on the radar image indicating the location of sandbanks or local shoals, which bring on wave breaking. This approach is practical merely in shallow coastal waters where bottom topography is of direct influence on wave breaking.

Note that radar systems are typically not capable of measuring environmental and atmospheric variables. Thus these variables have to be provided by external sources.

Supporting Sensors

Other remote sensing systems can also support the assessment of the probability of a detection being a spike. In literature, for example, measurements are described during which cameras and microphones were used to detect whitecaps and the noise of breaking waves respectively [8]. Although breaking waves and whitecapping are indeed prominent causes of sea spikes, other phenomena induce spiking events as well. These other phenomena, for instance microbreakers [4], may not be accompanied by whitecapping or loud noise. Thus the added value of cameras and microphones will be negligible. Furthermore, supportive sensors must be capable of measuring at the

maximum required range of 15 km.

In this study, the focus is on the possibilities of discriminating sea spikes from other detections by using radar data and in particular data from ordinary ship navigation radars. The use of information and measurements of external sources is outside the scope of this study.

3 The Ships Radar Concept

The Ships Radar (SHIRA) concept refers to the conceptual design and development of novel signal processing techniques for ship navigation radars [1]. With these techniques, standard navigation radars may be used for new applications such as the measurement of wave fields and currents or the detection of oil spills. The conceptual developments are prepared for operational use by TNO and SeaDarQ.

Ship navigation radars are generally basic, incoherent, single-polarized radar systems. They are equipped with a rotating antenna in order to image the area around the ship. The actual implementation of the navigation radar, used by TNO within the framework of SHIRA, was modified throughout the project. Modifications were made to, among others, the polarization, antenna length, and data acquisition. In the remainder of the report, the different implementations of the navigation radar will be simply referred to as 'SHIRA.'

Some standard system parameters of SHIRA are listed in Table 3.1. The transmitted pulse length, pulse repetition frequency (PRF), and sample rate are set by the operator before each measurement.

Table 3.1 Some standard SHIRA system parameters.

General Parameters			
Carrier Frequency:	9.4 GHz	Wavelength:	3.2 cm
PRF:	≤ 4 kHz	Pulse repetition interval (PRI):	≥ 0.25 ms
Short Pulse:	50 ns	Medium Pulse:	250 ns
Transmitted Power:	25 kW	Polarization:	HH or VV
Long Antenna Version			
Antenna Length:	3.66 m	Revolution Time:	1.6 s
Beamwidth:	0.5°	Angular Velocity:	$225^\circ/\text{s}$
Short Antenna Version			
Antenna Length:	1.83 m	Revolution Time:	1.2 s
Beamwidth:	1.0°	Angular Velocity:	$300^\circ/\text{s}$

Since SHIRA transmits unmodulated pulses, the range resolution depends on the pulse length

$$\delta r = \frac{c\tau}{2}, \quad (3.1)$$

in which c is the speed of light and τ is the pulse length. Thus the actual range resolution is either 7.5 m (short pulse) or 37.5 m (medium pulse). Note that the image pixel size is independent of the pulse length. In range direction, the pixel size is solely determined by the sample rate

$$\Delta R = \frac{c}{2f_s}, \quad (3.2)$$

where f_s is the sample frequency. Given the sample rate, the measurement range is determined by the number of samples recorded per range profile. The azimuth resolution depends on the antenna beamwidth

$$\delta x = \theta R, \quad (3.3)$$

with θ the antenna beamwidth and R the range. As can be seen, the azimuth resolution deteriorates as range increases. The nominal PRF of SHIRA is 1.2 kHz. Thus when the long antenna is used, the range profiles are separated in angle by around 0.2° . Since, the antenna beamwidth is 0.5° , the areas imaged by successive measurements overlap. Successive range profiles are therefore correlated.

In practice, the range profiles are not uniformly distributed in angle. The actual angular velocity of the antenna varies due to, for instance, wind fluctuations. As a consequence, the number of range profiles recorded per revolution varies. The angular position of the antenna is tracked by a counter in the radar processor. At regular angular increments, the antenna unit produces a digital pulse. The counter keeps track of the number of pulses in order to determine the antenna's angular position. The counter value or *absolute angle* is stored with each range profile [27].

For each completed revolution, the antenna unit produces a reset pulse, which is labeled *North reset* [1]. The North reset clears the counter. It should be noted that, although the label suggests differently, the North reset is not actually aligned with grid North.

3.1 Data Sets

Over the years, many experiments have been carried out with SHIRA, including experiments with small targets and dinghies. Unfortunately, most measurements were made at relatively short ranges; up to 6 km. Only few long-range data sets are available. Moreover, most SHIRA measurements are made with VV-polarization, with the result that sea spikes are less pronounced.

The process of selecting suitable data is further complicated by the fact that several system setups of SHIRA have been used throughout the years. No accurate record has been kept of the system setups or the measurement settings, such as PRF and transmitted pulse length. In principle, the system setup is specified in the file headers.

However, these headers have to be updated by hand after each system adjustment and are regrettably not reliable.

An overview of the finally selected data sets is given in Table 3.2. The actual SHIRA setup is listed as well as some weather and wave information when available².

An example image of each data set is shown in Figure 3.1. The images are roughly North-aligned by hand.

Data set 6 was especially recorded for this study; it is a long-range measurement with HH-polarization. However, during this measurement SHIRA was equipped with a short antenna with very poor performance. Therefore, data set 1 was selected to verify the processing algorithms to determine the dominant wave direction and period described in the next section. Unfortunately, it is a short-range data set, but it exhibits a very clear wave field that is a prerequisite for the algorithm verification. Furthermore, wave data from the Euro Platform are available for this day.

3.2 Discriminating Sea Spikes with SHIRA

In this section, the SHIRA signal processing will be discussed. The different processing steps will be visualized by means of data set 1, see Figure 3.2.

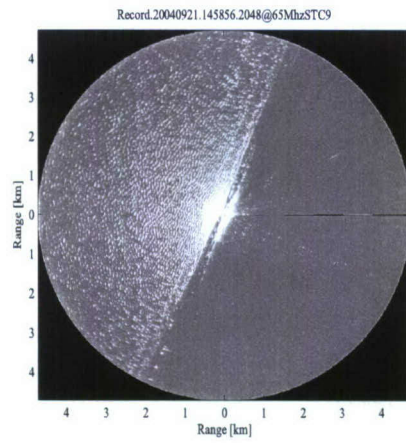
3.2.1 *Current Processing of Data Patches at Near-Range*

An important step in the near-range processing is the calculation of the wave spectrum to estimate the dominant wavelength, wave direction, and wave period. The wave spectrum is calculated by applying a two-dimensional fast Fourier transform (FFT) to a radar image. The use of an FFT necessitates the radar data to be available on a rectangular grid. The SHIRA data are however acquired on a polar grid, thus the first processing step is the interpolation of the radar data onto a rectangular grid. Currently, this interpolation is done with a basic nearest neighbor algorithm.

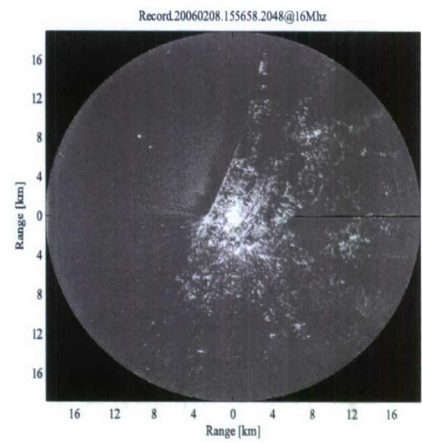
2. The weather information was obtained at the weather station near Rotterdam airport (located at 51° 57' N, 04° 27' E). The weather data are available online: <http://www.knmi.nl/>. The wave direction and period were obtained at the Euro Platform (located at 51° 59' N, 3° 16' E). The wave data are available online: <http://www.waterbase.nl/>. The wave direction is defined relative to grid North.

Table 3.2 SHIRA data selected for further analysis.

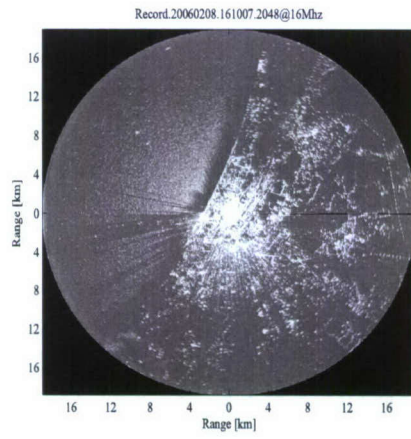
Data Set 1: Record.20040921.145856.2048@65MhzSTC9.drq		
Date & Location	System Parameters	Weather & Waves
September 21 st , 2004 Noordwijk (52° 14' N, 4° 26' E)	Long Antenna (VV) Short Pulse Sample Rate: 65 MHz No. Samples: 2048 Pixel Size ΔR : 2.3 m Range: 4.73 km	Heavy Clouding Temperature: 14.0 °C Wind Direction: W Wind Speed: 9.4 ms ⁻¹ Wave Direction: 290° Wave Period: 5.5 s
Data Set 2: Record.20060208.155658.2048@16Mhz.drq		
Date & Location	System Parameters	Weather
February 8 th , 2006 TNO, The Hague (52° 6' N, 4° 19' E)	Long Antenna (VV) Short Pulse Sample Rate: 16 MHz No. Samples: 2048 Pixel Size ΔR : 9.4 m Range: 19.20 km	Heavy Clouding Temperature: 5.0 °C Wind Direction: WNW Wind Speed: 8.5 ms ⁻¹
Data Set 3: Record.20060208.161007.2048@16Mhz.drq		
Date & Location	System Parameters	Weather
February 8 th , 2006 TNO, The Hague (52° 6' N, 4° 19' E)	Long Antenna (VV) Medium Pulse Sample Rate: 16 MHz No. Samples: 2048 Pixel Size ΔR : 9.4 m Range: 19.20 km	Heavy Clouding Temperature: 5.0 °C Wind Direction: WNW Wind Speed: 8.5 ms ⁻¹
Data Set 4: Toren.VV.20060209.100000.2048@22Mhz.drq		
Date & Location	System Parameters	Weather
February 9 th , 2006 TNO, The Hague (52° 6' N, 4° 19' E)	Long Antenna (VV) Short Pulse Sample Rate: 22 MHz No. Samples: 2048 Pixel Size ΔR : 6.8 m Range: 13.9 km	Cloudy/Heavy Clouding Temperature: 3.7 °C Wind Direction: NW Wind Speed: 8.4 ms ⁻¹
Data Set 5: Record.20060221.102114.2048@22Mhz.drq		
Date & Location	System Parameters	Weather & Waves
February 21 st , 2006 TNO, The Hague (52° 6' N, 4° 19' E)	Long Antenna (VV) Short Pulse Sample Rate: 22 MHz No. Samples: 2048 Pixel Size ΔR : 6.8 m Range: 13.9 km	Heavy Clouding Temperature: 3.1 °C Wind Direction: NE Wind Speed: 7.4 ms ⁻¹ Wave Direction: 19° Wave Period: 5.0 s
Data Set 6: Record.20061031.140930.4096@16mhz.drq		
Date & Location	System Parameters	Weather
October 31 st , 2006 TNO, The Hague (52° 6' N, 4° 19' E)	Short Antenna (HH) Short Pulse Sample Rate: 16 MHz No. Samples: 4096 Pixel Size ΔR : 9.4 m Range: 38.40 km	Heavy Clouding Temperature: 12.9 °C Wind Direction: W Wind Speed: 8.2 ms ⁻¹



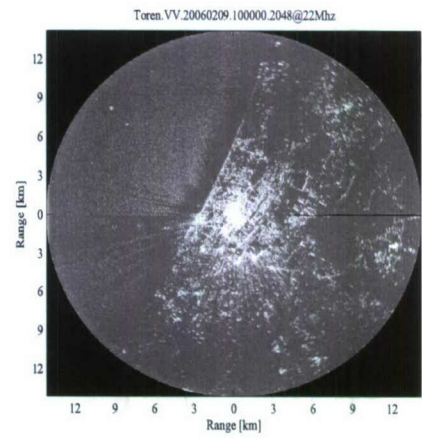
(a) Set 1; September 21st 2004, Noordwijk.



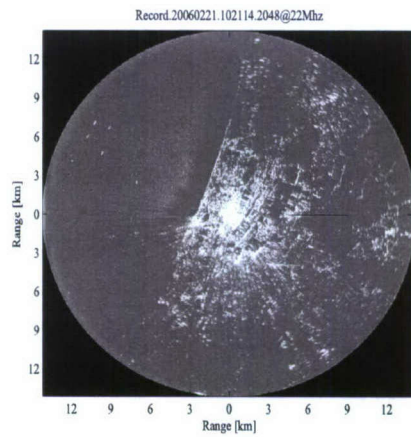
(b) Set 2; February 8th 2006, The Hague.



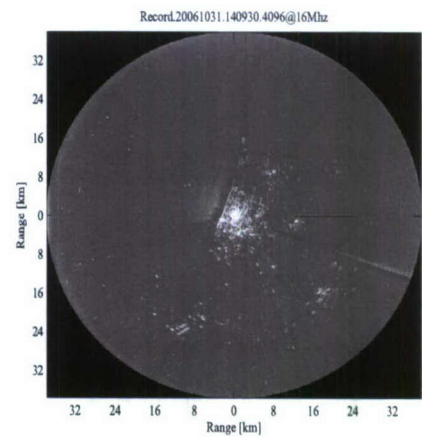
(c) Set 3; February 8th 2006, The Hague.



(d) Set 4; February 9th 2006, The Hague.



(e) Set 5; February 21st 2006, The Hague.



(f) Set 6; October 31st 2006, The Hague.

Figure 3.1 Overview of selected SHIRA data sets.

A disadvantage of this algorithm is that it affects the data; there is no preservation of energy. Moreover, successive range profiles are correlated, which is not taken into account during the interpolation (the beamwidth in azimuth is 0.5° , whereas the angle between two measurements is of the order of 0.2° depending on the PRF). Therefore, the process of interpolation may affect the statistics of the radar data, which in turn may degrade the performance of a CFAR detector.

That the nearest neighbors interpolation indeed affects the radar data is shown in Figure 3.3. In this figure, spatial wave spectra obtained from different areas are shown. A detector has been applied to the wave spectra, the detections are shown as white pixels. As can be seen, the location of the selected area (around the y -axis, x -axis, or $x = y$ axis) influences the wave spectrum, especially for higher wave numbers. This is in accordance with a study conducted earlier in the SHIRA program to investigate the effects of interpolation [28]. Nevertheless, in this study it was concluded that the dominant wavelength and wave direction can be reliably estimated, since the spectra are not degraded for lower wave numbers.

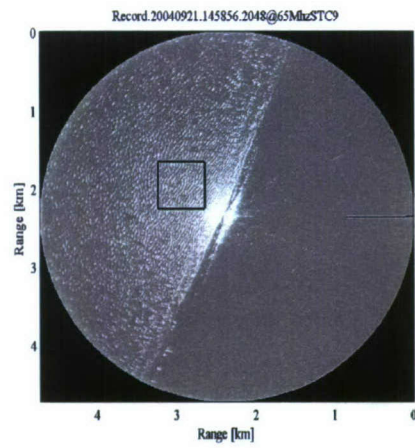
After the interpolation, a patch of data at relatively short range ($R < 3$ km) is selected to calculate the wave spectrum, see Figure 3.2(a). The selected area should exhibit a clear wave field in order to obtain a reliable estimate of the dominant wave parameters. As can be seen in Figure 3.2(b), the selected patch at short range indeed shows a clear wave field. Subsequently, the 2-dimensional spatial wave spectrum is calculated and with the aid of a CFAR detector the dominant wave direction and wavelength are determined. The wave spectrum is shown in Figure 3.2(c); the CFAR detections are presented by white pixels. The dominant wave direction and wavelength are obtained by calculating a weighted average of the CFAR detections; they are indicated by the red diamonds. Note that the detections at very short ($\lambda < 40$ m) and very long ($\lambda > 150$ m) wavelengths are not taken into account in the weighted average. Thus the noise induced by the nearest neighbor interpolation is filtered out. The calculated wavelength is around 72 m, which is a common value for the North Sea, and the wave direction is 298° , which corresponds very well to the 290° measured by the Euro Platform (especially considering that the data were North-aligned by hand).

By tracking the phase of the dominant wave from rotation to rotation, the wave period can be determined. The resulting temporal frequency spectrum is shown in Figure 3.2(d). The calculated wave period is 8.3 s, which deviates from the 5.5 s measured by the Euro Platform. This is in contrast with the assumption that the wave parameters are stationary over large areas of the sea. Most likely, this is due to the fact that the measurements are made in shallow coastal waters instead of the open ocean. Consequently, a patch of data is selected at larger range. The signal processing of this large-range patch will be described in the following section.

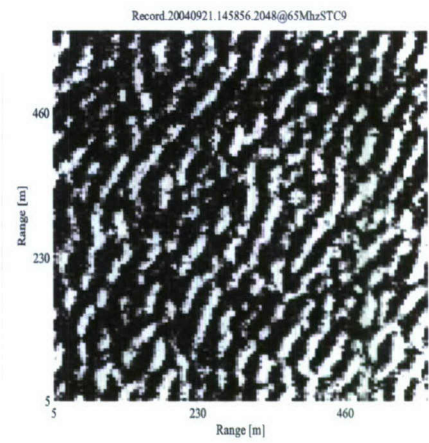
3.2.2 *Processing of Data Patches at Long-Range*

When the wave parameters are estimated for a patch of data at near range, an area is selected at larger range, see Figure 3.2(e). A detailed image of the selected area is presented in Figure 3.2(f). The spiky nature of the sea clutter, compared to the near-range image shown in Figure 3.2(b), is apparent. Since the long-range patch lacks a clear continuous wave field, it is not feasible to obtain reliable estimates of the wave parameters from this patch.

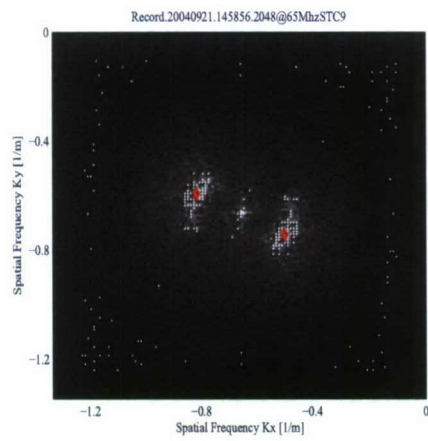
Nevertheless, a CFAR detector and subsequently a cluster algorithm can be applied to the long-range data patch. In the following paragraphs, the possibilities of isolating sea spikes within SHIRA data will be assessed (refer also to the discussion in Section 2.5).



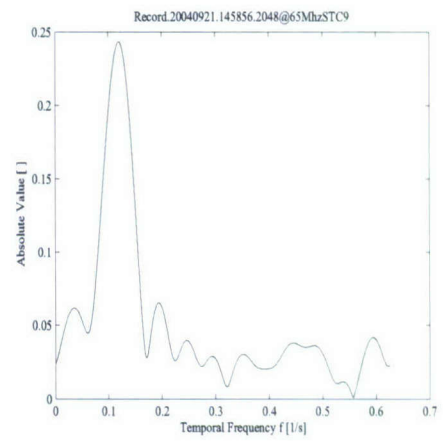
(a) Data set 1; selected area at short range.



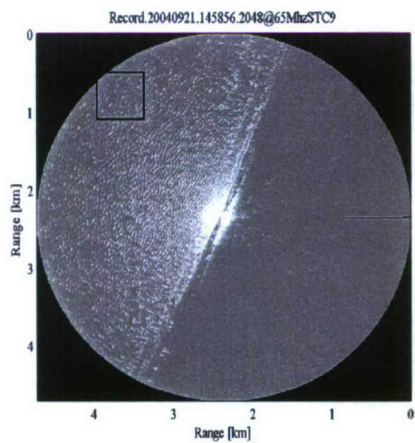
(b) Image of the selected area at short range.



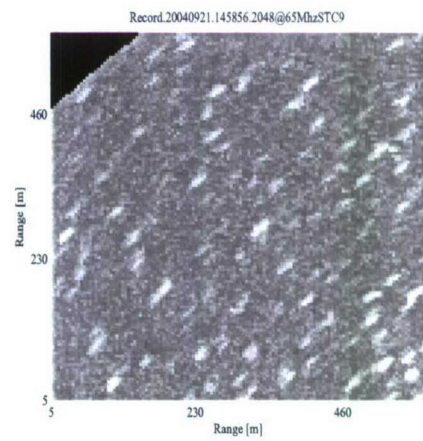
(c) The wave spatial spectrum.



(d) The wave temporal spectrum.

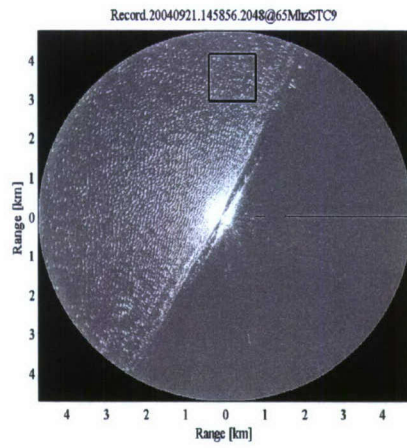


(e) Data set 1; selected area at larger range.

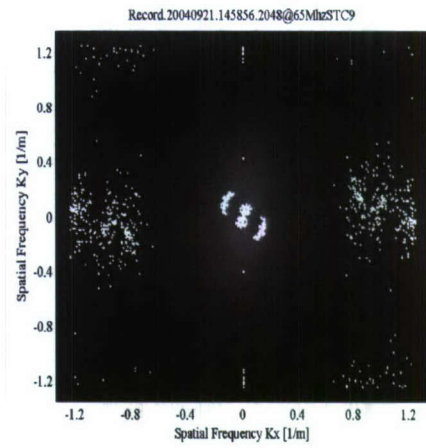


(f) Image of the selected area at larger range.

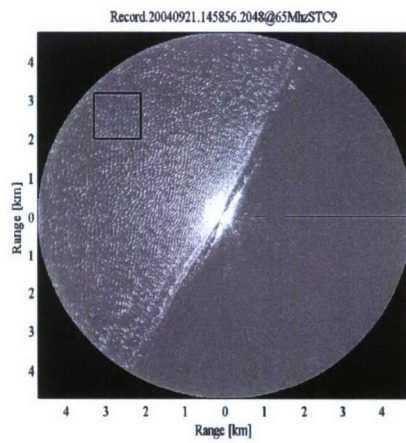
Figure 3.2 Overview of the successive SHIRA signal processing steps.



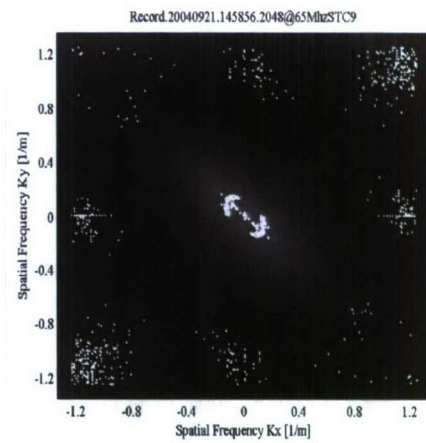
(a) Selected area around the y -axis.



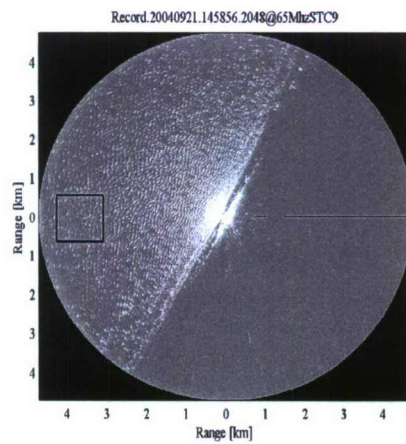
(b) Corresponding wave spectrum.



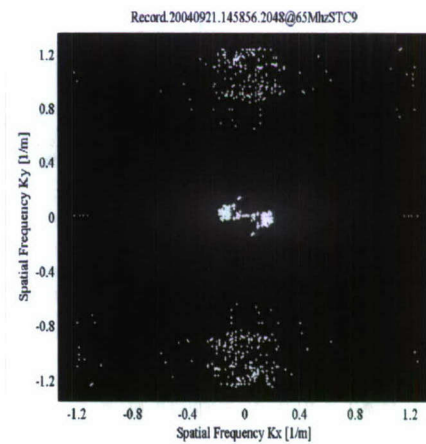
(c) Selected area around the $x = y$ axis.



(d) Corresponding wave spectrum.



(e) Selected area around the x -axis.



(f) Corresponding wave spectrum.

Figure 3.3 The effect of the nearest neighbor interpolation on the calculated 2-dimensional spatial wave spectrum.

Statistical, Polarimetric, and Doppler Properties

The CFAR detector presently applied in the SHIRA processing is based on Gaussian distributed clutter. As was shown in Section 2.4, the performance of a CFAR detector improves when more appropriate sea clutter statistics are used.

Obviously, polarimetric and Doppler properties cannot be measured with a basic incoherent, single-polarized navigation radar, such as SHIRA.

Spatial and Temporal Correlation

The velocity and direction of propagation of the clusters can be estimated when the clusters are tracked from rotation to rotation. Subsequently, the motion and orientation of the clusters can be compared to the wave direction and wave period estimated from the near-range data. This comparison is however only meaningful when the wave parameters are stationary over large areas of the ocean. Especially in shallow littoral waters this is not true.

The comparison is furthermore complicated by the short lifetime of spiking events.

The wave-breaking process takes place in a very short time, generally within a quarter of the wave period [29]; i.e. 2 to 3 s. The rotation time of SHIRA is of the order of 1.5 s.

Thus SHIRA can collect only one or maybe two detections of a spiking event, which is too little to construct a reliable track and measure the distinct properties required for the comparison.

Thus summarizing the above, the performance of SHIRA can be improved by optimizing the CFAR detector with respect to the amplitude distribution of sea clutter. The implementation of an adapted CFAR is straightforward, i.e. it has no impact on the radar hardware.

4 Conclusion

One of the goals of this research was to assess the possibilities that may exist for the detection of small targets in clutter-contaminated radar observations of the sea surface. The main focus is on the region between 5 and 15 km from the radar. At these rather long ranges, the HH-polarized radar backscatter is dominated by sea spikes. Spiking events may result from several processes. The most prominent is wave breaking, but also steep and highly curved patches of ocean surface can lead to strong reflections that manifest themselves as sea spikes. Different percentages of breaking and non-breaking waves leading to sea spike observations are reported, ranging roughly between 30% and 80%.

A literature search has resulted in a multitude of observational studies. Most of these, however, focus on sets of measurements from either wavetanks or single locations. Statistics on sea spike behavior are representative of a particular dataset, but cannot be generalized. Local conditions of wind, local and remote wave field characteristics, and shore and bottom topography strongly influence the results, but their influence is unpredictable mainly due to indeterminate correlations. Rapid progress in the development of sea spike classification techniques is therefore not expected from a prediction of sea spike density based on environmental quantities.

A statistical approach towards an improved description of the distribution underlying the spiky scatter may provide some benefit. At high grazing angles and low resolution, the sea clutter amplitude has a Rayleigh distribution. For high resolution radar at low grazing angles, the amplitude becomes quickly less Rayleigh distributed and the high-backscatter tail of the distribution grows, as well as the variance to mean ratio. The detection algorithms currently applied in SHIRA use a CFAR technique based on Rayleigh distributed signals. Some benefit is expected from using a more appropriate distribution model for the sea clutter. Some of the more widely used distribution models for spiky sea clutter are the Weibull, log-normal and K -distributions. A comparison of CFAR detectors using measured data showed that a 'Weibull detector' does indeed perform better than a 'Gaussian detector.' Nevertheless, the false-alarm rate remains too high.

It is improbable that small targets can be detected at distances ranging from 5 to 15 km at a reasonable false-alarm rate when sea spikes cannot be distinguished from true target echoes. Such a distinction may be made by exploiting the particular properties of sea spikes. The most distinctive properties of spiking events are the sudden increase in Doppler speed and polarization ratio. These properties cannot be measured with standard incoherent navigation radars.

At present, coherent navigation radars are being developed [30]. Therefore, it is worthwhile to investigate the value of using coherent data in the classification process. Such an investigation may start with a literature research focused on coherent radar observations of sea clutter and small targets. Subsequently, special classification techniques exploiting Doppler characteristics of sea spikes can be developed. However, for the development and validation of novel classification techniques the availability of coherent sea clutter data, preferably with some small targets present, is mandatory.

5 References

- [1] J. C. M. Kleijweg, R. J. P. van Bree, R. A. van Maarseveen, A. J. E. Smith, "DEKODO/REA Gebruik van een navigatieradar voor detectie van kleine oppervlakte doelen en rapid environmental assessment," TNO, The Hague, The Netherlands, Tech. Rep. TNO-DV 2007 A354, December 2007.
- [2] H. Greidanus, "An Implemented Bragg-based Model for High Resolution Radar Sea Clutter," TNO, The Hague, The Netherlands, Tech. Rep. TNO-DV1 2003 A039, January 2005.
- [3] H. W. Melief, H. Greidanus, P. van Genderen, and P. Hoogetboom, "Analysis of Sea Spikes in Radar Sea Clutter Data," *IEEE Trans. Geosci. Remote Sensing*, vol. 44, no. 4, pp. 985-993, 2006.
- [4] H. W. Melief, "Dynamic Modelling of Radar Seaclutter," Delft University of Technology, Delft, The Netherlands, Dissertation, November 2006.
- [5] R. J. P. van Bree, "V-Wake Detection with a Navigational Radar," TNO, The Hague, The Netherlands, Tech. Rep. TNO-DV1 2005 B183, 2005.
- [6] R. J. P. van Bree, "V-Wake Detection with a Navigational Radar: Results," TNO, The Hague, The Netherlands, Tech. Rep. TNO-DV1 2006 B388, December 2006.
- [7] H. Greidanus, H. W. Melief, P. Hoogetboom, and P. van Genderen, "Doppler Polarimetry of High Resolution Radar Sea Clutter," in *Proc. IGARSS*, Sydney, Australia, July 9-13, 2001.
- [8] Y. Liu, J. F. Frasier, and R. E. McIntosh, "Measurement and Classification of Low-Grazing-Angle Radar Sea Spikes," *IEEE Trans. Antennas propagat.*, vol. 46, no. 1, pp. 27-40, Jan. 1998.
- [9] J. C. West, "Ray Analysis of Low-Grazing Scattering from a Breaking Wave," *IEEE Trans. Geosci. Remote Sensing*, vol. 37, no. 6, pp. 2725-2727, Nov. 1999.
- [10] E.A. Ericson, D. R. Lyzenga, and D. T. Walker, "Radar Backscatter from Stationary Breaking Waves," *J. Geophys. Res.*, vol. 104, no. C12, pp. 29679-29695, 1999.
- [11] P. Bonmarin, "Geometric Properties of Deep-Water Breaking Waves," *J. Fluid Mech.*, vol. 209, pp. 405-433, 1989.
- [12] J. Fuchs, D. Regas, T. Waseda, S. Welch, and M. P. Tulin, "Correlation of Hydrodynamic Features with LGA Radar Backscatter from Breaking Waves," *IEEE Trans. Geosci. Remote Sensing*, vol. 37, no. 5, pp. 2442-2460, 1999.
- [13] M. I. Skolnik, *Introduction to Radar Systems*. London: McGraw-Hill, 1980, pp. 477.
- [14] Y. Dong, "Distribution of X-Band High Resolution and High Grazing Angle Sea Clutter," DSTO, Edinburgh, Australia, Tech. Rep. DSTO-RR-0316, July 2006.
- [15] H. Dankert, J. Horstmann, and W. Rosenthal, "Ocean Wind Fields Retrieved from Radar-Image Sequences," *J. Geophys. Res.*, no. 108, 2003.
- [16] D. Walker, "Doppler Modelling of Radar Sea Clutter," *IEE Proc. Radar Sonar Navig.*, vol. 148, no. 2, pp. 73-80, 2001.
- [17] M. R. Keller, B. L. Gotwols, and R. Chapman, "Sea Spikes at Moderate to Near Grazing Incidence Angles," presented at the IEEE AP-S Int. Symp. and USNC/URSI National Radio Science Meeting, Boston, U.S.A., July 8-13, 2001.
- [18] T. J. Nohara and S. Haykin, "Canadian East Coast Radar Trials and the K-Distribution," *IEE Proc. Pt. F*, vol. 138, no. 2, pp. 80-88, 1991.
- [19] M. I. Skolnik, *Introduction to Radar Systems*. London: McGraw-Hill, 1980, pp. 478.

- [20] B. L. Gotwols, R. D. Chapman, and D. R. Thompson, "Doppler Spectra and Backscatter Cross Section Over 45°-85° Incidence," in *Proc. NATO/RTO Symp. Low Grazing Angle Clutter, Characterization, Measurement and Application*, Laurel, U.S.A., April 25-27, 2000.
- [21] I. Antipov, "Analysis of Sea Clutter Data," DSTO, Salisbury, Australia, Tech. Rep. DSTO-TR-0647, March 1998.
- [22] I. Antipov, "Statistical Analysis of Northern Australian Coastline Sea Clutter Data," DSTO, Edinburgh, Australia, Tech. Rep. DSTO-TR-1236, November 2001.
- [23] N. J. Redding, "Estimating the Parameters of the K -Distribution in the Intensity Domain," DSTO, Salisbury, Australia, Tech. Rep. DSTO-TR-0839, July 1999.
- [24] H. W. Melief, H. Greidanus, and H. J. M. Heemskerk, "Analysis of High Resolution Coherent Polarized Sea Clutter Data at Low Grazing Angles," TNO, The Hague, The Netherlands, Tech. Rep. FEL-01-A216, September 2001.
- [25] M. J. Smith, E. M. Poulter, and J. A. McGregor, "Doppler Radar Measurements of Wave Groups and Breaking Waves," *J. Geophys. Res.*, vol. 101, no. C6, pp. 14269-14282, 1996.
- [26] R. J. A. Tough, K. D. Ward, and W. P. Shepherd, "The Modelling and Exploitation of Spatial Correlation in Spiky Sea Clutter," in *Proc. 2nd European Radar Conf.*, Paris, France, Oct. 6-7, 2005.
- [27] A. Verburgt, "SeaDarQ Data Format," TNO, The Hague, The Netherlands, Tech. Note, February 2005.
- [28] J. van de Laar, "Ship's Radar Data Acquisition System and Polar Spectral Analysis of Sea Wave Patterns," TU Eindhoven, Eindhoven, The Netherlands, Tech. Rep. SPS 11-00, August 2000.
- [29] P. Wang, Y. Yao, and M. P. Tulin, "An Efficient Numerical Tank for Non-Linear Water Waves, based on the Multi-Subdomain Approach with BEM," *Int. J. Numerical Methods Fluids*, vol. 20, no. 12, pp. 1315-1335, 1995.
- [30] B. Wade, "SHARPEYE a 'New Technology' Marine Radar," in *Proc. IET Radar*, Edinburgh, U.K., October 15-18, 2007.

Signature

The Hague, March 2008

TNO Defence, Security and Safety



J.P. Dezaire, MSc
Head of department



Dr J.J.M. de Wit, MSc
Author

ONGERUBRICEERD
REPORT DOCUMENTATION PAGE
(MOD-NL)

1. DEFENCE REPORT NO (MOD-NL) TD2008-0023	2. RECIPIENT'S ACCESSION NO	3. PERFORMING ORGANIZATION REPORT NO TNO-DV 2008 A067
4. PROJECT/TASK/WORK UNIT NO 032-10287	5. CONTRACT NO -	6. REPORT DATE February 2008
7. NUMBER OF PAGES 33 (excl RDP & distribution list)	8. NUMBER OF REFERENCES 30	9. TYPE OF REPORT AND DATES COVERED Final
10. TITLE AND SUBTITLE Discriminating Sea Spikes in Incoherent Radar Measurements of Sea Clutter		
11. AUTHOR(S) Dr J. J. M. de Wit, MSc Dr M. W. Schouten, MSc		
12. PERFORMING ORGANIZATION NAME(S) AND ADDRESS(ES) TNO Defence, Security and Safety, P.O. Box 96864, 2509 JG The Hague, The Netherlands Oude Waalsdorperweg 63, The Hague, The Netherlands		
13. SPONSORING AGENCY NAME(S) AND ADDRESS(ES) Royal Netherlands Navy, Defence Material Organization P.O. Box 20702, 2500 ES The Hague, The Netherlands		
14. SUPPLEMENTARY NOTES The classification designation Ongerubricenseerd is equivalent to Unclassified, Stg. Confidentieel is equivalent to Confidential and Stg. Geheim is equivalent to Secret.		
15. ABSTRACT (MAXIMUM 200 WORDS (1044 BYTE)) In this report, the results of an inventory of sea spike characteristics is given. Furthermore, the possibility to detect sea spikes with standard ship navigation radars is explored. In literature it was found that the most distinct properties of sea spikes are the sudden increase in polarization ratio HH/VV and Doppler velocity. These properties cannot be measured with current navigation radars, but future navigation radars will be coherent. It is therefore worthwhile to investigate the added value of using coherent sea clutter data in the sea spike detection and classification process.		
16. DESCRIPTORS Shipborne Radar, Target Detection, Sea Clutter, Navigation	IDENTIFIERS Small Vessels, SHIRA, Sea Spikes	
17a. SECURITY CLASSIFICATION (OF REPORT) Ongerubricenseerd	17b. SECURITY CLASSIFICATION (OF PAGE) Ongerubricenseerd	17c. SECURITY CLASSIFICATION (OF ABSTRACT) Ongerubricenseerd
18. DISTRIBUTION AVAILABILITY STATEMENT Unlimited	17d. SECURITY CLASSIFICATION (OF TITLES) Ongerubricenseerd	

ONGERUBRICEERD

Distribution list

The following agencies/people will receive a complete copy of the report.

- | | |
|-------|---|
| 1 | DMO/SC-DR&D |
| 2/3 | DMO/DR&D/Kennistransfer |
| 4 | Programmabegeleider Defensie
drs. W. Pelt |
| 5/7 | Bibliotheek KMA |
| 8 | Bibliotheek KIM |
| 9 | KIM, Prof F. Absil |
| 10 | DOBBP, afdeling Marinebehoeften |
| 11 | CZSK, drs J. Muys |
| 12 | DMO/Wapensystemen, Hoofd bureau Sensoren |
| 13 | DMO/Wapensystemen/Sensoren,
ir. O. Zeijpveld |
| 14 | Marinebedrijf/Advies |
| 15 | Bibliotheek KNMI |
| 16 | Programmaleider TNO Defensie en Veiligheid,
dr. A.M.J. van Eijk |
| 17/20 | TNO Defensie en Veiligheid, vestiging Den Haag,
Business Unit Waarnemingsystemen,
drs. J.S. Groot
ir. J.C.M. Kleijweg
dr. ir. M.W. Schouten
dr. ir. J.J.M de Wit |

Onderstaande instanties/personen ontvangen het managementuittreksel en de distributielijst van het rapport.

- 4 ex. DMO/SC-DR&D
- 1 ex. DMO/ressort Zeesystemen
- 1 ex. DMO/ressort Landsystemen
- 1 ex. DMO/ressort Luchtsystemen
- 2 ex. BS/DS/DOBBP/SCOB
- 1 ex. MIVD/AAR/BMT
- 1 ex. Staf CZSK
- 1 ex. Staf CLAS
- 1 ex. Staf CLSK
- 1 ex. Staf KMar
- 1 ex. TNO Defensie en Veiligheid, Algemeen Directeur,
ir. P.A.O.G. Korting
- 1 ex. TNO Defensie en Veiligheid, Directie
Directeur Operaties, ir. C. Eberwijn
- 1 ex. TNO Defensie en Veiligheid, Directie
Directeur Kennis, prof. dr. P. Werkhoven
- 1 ex. TNO Defensie en Veiligheid, Directie
Directeur Markt, G.D. Klein Baltink
- 1 ex. TNO Defensie en Veiligheid, vestiging Den Haag,
Manager Waarnemingssystemen (operaties), ir. B. Dunnebier PDeng
- 1 ex. TNO Defensie en Veiligheid, vestiging Den Haag,
Manager Informatie en Operaties (operaties), ir. P. Schulein
- 1 ex. TNO Defensie en Veiligheid, vestiging Rijswijk, daarna reserve
Manager Bescherming, Munitie en Wapens (operaties), ir. P.J.M. Elands
- 1 ex. TNO Defensie en Veiligheid, vestiging Rijswijk,
Manager BC Bescherming (operaties), ir. R.J.A. Kersten
- 1 ex. TNO Defensie en Veiligheid, vestiging Soesterberg,
Manager Human Factors (operaties), drs. H.J. Vink